Minimally Invasive Tumour Ablation Model

by Sheldon Hall

MITA models user guide.

Table of contents

Minimally invasive tumour ablation (MITA) therapies involve the placement of one or more applicators in close proximity to a tumour under image guidance. This can be done either percutaneously or laparoscopically to avoid open surgery and the related risks and comorbities. A variety of modalities are available: microwave ablation, radiofrequency ablation, cryoablation, laser ablation and irreversible electroporation. Once the applicator(s) have been positioned they are resonsible for generating or removing heat or inducing a pulsed electric field to produce a coagulation zone encompassing the tumour.

The mathematical models describing these MITA therapies can all be solved in FEniCS, and due to the similarities in the underlying equations and solution methods, it is advantageous to collect them in a single application. Models of MITA therapies can be broken into three main constituents: a model of the action of the applicator (eg: microwave antenna); a model of the heat transfer in the tissue (eq: bioheat equation); and a model for cell death as a result of the procedure. These three components form a coupled nonlinear system of equations, commonly seen in multiphysics applications.

The use of the bioheat equation is shared by most MITA models, and therefore it makes sense to develop a single model, applicable to all, that can be reused without having to repeat all of the code verification and validation for each modality.

1 Getting Started

This code relies on the programs git, FEniCS, Python, GMSH and MatLab being installed and configured in advance. This is most easily achieved on a system running Ubuntu 10.04 LTS, which is the code development platform. The code is contained in a git repository (distributed version control http://git-scm.com/) and the latest release can be obtained by cloning the repository to a local machine using the command line:

cd "directory"
git clone https://github.com/sheldonkhall/MITA-model.git

where "directory" is the desired installation directory. Once this has been done the install script should be run by issuing the command:

./install.sh

The install script currently uses GMSH to generate the meshes for the test cases and converts them to the FEniCS file format using dolfin-convert.

In order to run the test cases provided, the following command should be issued on the command line from the installation directory:

python "filename".py

where "filename" should be replaced with one of the test cases described in Sec. 4. All tests can be run at once using the script run_tests.sh to check an installation.

1.1 Mesh Generation

All of the test cases include mesh files created using GMSH, an open-source finite element grid generator. To identify relevant boundaries and subdomains for the solver GMSH can be used to tag certain parts of the domain with integers. This is done by defining physical surfaces and lines before generating the mesh. Parameters can then be set in the input file to inform the solver.

2 Code Structure

The most complex component of the code, utilised in modelling all modalities, is the effective heat capacity form of Pennes equation. This is a nonlinear PDE solver that is coupled to the other components, e.g. cell death model, in specific combinations to form the models of each modality. For this reason the core component of this code is the solver for Pennes equation, which calls the other components as required. The other components can all be called in isolation for static solutions, but in order to obtain a transient solution to the full system of equations the framework in the Pennes equation solver must be utilised. This is illustrated in Fig. 1.
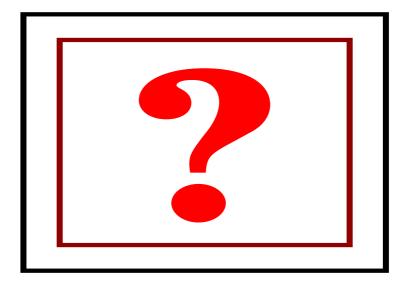
Figure 1. Schematic of the code highlighting the importance of the Pennes equation solver. The information being passed between the components is given explicitly: T is the temperature, V is the cell viability and SAR the specific absorption rate.

3 Code Components

In this section the determining equations for each model component are detailed for reference. The relevant code parameters are also defined.

3.1 Apparent heat capacity form of the Pennes equation

In order to compute the evolution of the system over time, including the dominant physical processes, the apparent heat capacity form of the Pennes equation is solved. This is given by:

$$\rho c_{\mathrm{app}}(T)\frac{\partial T}{\partial t} = \boldsymbol{\nabla} \cdot k(T)\boldsymbol{\nabla}T - \omega_b(T)\, c_b[T - T_0] + Q(T),$$

where T is the temperature in K, k is the thermal conductivity, ω_b is the blood perfusion in kg/s/m^3, c_b is the specific heat capacity of blood in J/kg/K, T_0 is the arterial blood temperature taken to be 310K and Q is the heat source generated by the probe in W/m^3. The effective specific heat, ρc_{app}, is given by:

$$\rho c_{\mathrm{app}} = \begin{cases} \rho c & T \leq T_l \\ \frac{\rho c + \rho_{\mathrm{vap}}\, c_{\mathrm{vap}}}{2} + \rho_w\, L\, C\, \frac{1}{T_u - T_l} & T_l < T \leq T_u \\ \rho_{\mathrm{vap}}\, c_{\mathrm{vap}} & T_u < T \end{cases},$$

where ρ and ρ_{vap} are the density (kg/m^3) of normal and vapourised tissue respectively, c and c_{vap} are the specific heat (J/kg/K) of normal and vapourised tissue respectively, ρ_w is the density of water, L is the latent heat of vapourisation (J/kg), C is the tissue water fraction. Water is assumed to be released from the tissue over a range of temperatures defined by $T \in [T_l, T_u]$, as is expected in mixtures.

To set the various parameters in this model see Tab. 1.

Symbol	Variable Name	Default Value
ρc	rho_c_t	1060 x 3411
$\rho_{\mathrm{vap}} c_{\mathrm{vap}}$	rho_c_v	4.4e5
$\rho_w L$	Lh	2260.0e3
C	Cliq	0.8
T_u	Tu	373
T_l	Tl	363
c_b	c	3640

Table 1.

All other parameters are dependent on a state variables and are treated separately.

3.1.1 Thermal conductivity k

The thermal conductivity is set to a constant value thp.k by default, which is commonly used in the literature [6] due to the limited impact on the results. For the purpose of the sensitivity analysis a linear temperature dependence has been introduced, which is selected by setting thp.k_method = "linear". This sets

$$k = k_0 + \Delta k[T - T_0],$$

where k_0 is the baseline thermal conductivity, Δk is the change in k per Kelvin and T_0 is the reference temperature at which k_0 has been measured (set to thp.T0 by default).

When considering phase change the functional form of k must be valid at $T > 373$K. In order to do this a piecewise continuous function is used

$$k(T) = \begin{cases} k_0 + \Delta k[T - T_0] & T \leq 373K \\ k_0 + \Delta k[373 - T_0] & T > 373K \end{cases}.$$

This is selected by setting thp.k_method = "linear_limited".

3.1.2 Steady-state temperature

In order to compute a steady-state solution of the Pennes equation, which is useful for benchmarking, a few parameter values must be set. These are summarised in the table below:

Parameter	Value
thp.rho_c_t	0.
thp.rho_c_v	0.
dt	a>0.
dt_min	a
dt_max	a
tmax	a
t_out	a
thp.perf_model	"constant"
thp.k_method	"constant"
thp.em_method	"custom"
thp.stop_on_me	False

Table 2.

There is an example of this in the mms-heat-only-test.py file.

3.2 Electric Potential Solver (RFA)

In order to determine the heat deposited by the probe, a simplified form of Maxwell's equations can be solved. Due to the large difference in the timescales of the electrical and thermal problems a quasi-static approximation can be made and a solution found in terms of the electric potential V determined by:

$$\boldsymbol{\nabla} \cdot \sigma(T) \boldsymbol{\nabla} V = 0,$$

where σ is the electrical conductivity. This is subject to dirichlet boundary conditions on the probe surface and on the external surfaces. The probe voltage is set in emp.Vprobe, and the external surface voltage in emp.V0 which establishes a potential difference similar to that between the probe and ground pads in a patient. This drives a current through the tissue resulting in resistive heating. The generated heat can be computed using:

$$\mathrm{SAR} = \sigma(T)|\boldsymbol{\nabla} V|^2.$$

3.2.1 Electrical conductivity σ

The electrical conductivity is set to a constant value by default and can be adjusted by setting emp.cond. A more realistic linear function of temperature is also available:

$$\sigma(T) = \sigma_0 + \Delta\sigma[T - T_0],$$

where σ_0 is the baseline conductivity, $\Delta\sigma$ is the change in the conduvitvity per Kelvin and T_0 is the reference temperature at which σ_0 has been measured (set to thp.T0 by default). This can be selected by setting emp.cond_model = "linear".

When considering phase change the functional form of σ must be valid at $T > 373\mathrm{K}$. In order to do this a piecewise continuous function is used

$$\sigma(T) = \begin{cases} \sigma_0 + \Delta\sigma[T - T_0] & T \leq T_u \\ [\sigma_{\mathrm{vap}} - [\sigma_0 + \Delta\sigma[T_u - T_0]]][T - T_u]/5 + \sigma_0 + \Delta\sigma[T_u - T_0] & T_u < T \leq T_u + 5 \\ \sigma_{\mathrm{vap}} & T_u + 5 < T \end{cases},$$

where This is selected by setting thp.k_method = "nonlinear".

3.2.2 Control System

Commercial RFA systems are controlled by adjusting the applied voltage to ensure either: the deposited power remains constant; the maximum temperature is never exceeded; or the impedance does not cross a threshold indicating extensive vapourisation [2].

Impedance

When the impedance specified in emp.imp_max is exceeded the calculation of the SAR is stopped for a period of emp.imp_t_off s [?]. The flag imp_on reflects whether or not the SAR will be computed for time t.

3.2.3 Computation of useful quantities.

The impedance of the tissue between the probe and the ground pads is an ideal indicator of the presence of vapourisation near the probe surface. For this reason it is used to control the power deposition during RFA. An impedance threshold is chosen; above which the generator is halted to allow the tissue to cool and any generated gas to dissipate from the near vicinity of the probe. In the EQS approximation being used to compute the potential, the resistance can be computed using:

$$R(t) = \frac{V(t)}{P_{\mathrm{total}}(t)},$$

where $R(t)$ is the resistance, $V(t)$ is the applied voltage and $P_{\mathrm{total}(t)}$ the power deposited in the tissue. $P_{\mathrm{total}}(t)$ is computed from the SAR by integrating over the computational domain(Kroger):

$$P_{\mathrm{total}}(t) = \int \mathrm{SAR}(t, \boldsymbol{r})\ \mathrm{dV}.$$

In the axisymmetric cylindrical coordinate system commonly used for these computations the equivalent form of the integral is:

$$P_{\mathrm{total}}(t) = 2\pi \iiint \mathrm{SAR}(t, \boldsymbol{r})\ r\ \mathrm{dr}\ \mathrm{dz}.$$

3.3 Vector Helmholtz Solver (MWA)

The literature, mostly composed of COMSOL models, indicates that in the axisymmetric case, in cylindrical coordinates, Maxwell's Equations simplify significantly. The problem reduces to that of finding a scalar field in two spacial dimensions [1]. Unfortunately in 3D there is no such simplification and the Vector Helmholtz or curl curl form must be solved. The advantage of dealing with a microwave system driven at a single frequency with "simple" materials however, is that system of equations can be solved in the frequency domain. This removes the complications related with computing the eigenvalues and eigenmodes.

3.3.1 Scalar Form

Suppose $\boldsymbol{H}$ defines the magnetic field over a domain Ω. We assume $\boldsymbol{H}(\boldsymbol{r},\,t) = \boldsymbol{H}(r,\,z,\,t)$ is axisymmetric and that $\boldsymbol{H}(\boldsymbol{r},t) = \left(0, \tilde{H}_\phi, 0\right)$ in cylindrical coordinates. We further assume that $\boldsymbol{H}$ is time-harmonic, that is we can define an H_ϕ such that $\tilde{H}_\phi(\boldsymbol{r},t) = H_\phi(\boldsymbol{r})\cos\left(\omega\,t + \alpha\right)$. We take $\alpha = 0$, without loss of generality. In the frequency domain, it is possible to model a lossy medium by considering a complex-valued permittivity - $\varepsilon_r = \varepsilon_r' - j\varepsilon_r''$ - this accounts for the non-local nature of the dispersive model. However, this means we must also consider H_ϕ as a map to the complex domain.

From Gas [1] (of the COMSOL family),

$$\nabla \times \left[\left(\varepsilon_r - j\,\frac{\sigma}{\omega\,\varepsilon_0}\right)^{-1} \nabla \times \boldsymbol{H}\right] - \mu_r\,k_0^2\,\boldsymbol{H} = 0 \tag{1}$$

Then,

$$\nabla \times \boldsymbol{H} = \left[\left(-\frac{\partial}{\partial z}H_\phi\right)\boldsymbol{e}_r + \left(\frac{1}{r}\frac{\partial}{\partial r}\left(r\,H_\phi\right)\right)\boldsymbol{e}_z\right], \tag{2}$$

Using 2 we can expand,

$$\nabla \times \hat{\varepsilon_r}(\nabla \times \boldsymbol{H}) = \left[\frac{1}{r}\frac{\partial}{\partial\phi}\left(\frac{\hat{\varepsilon_r}}{r}\frac{\partial}{\partial r}\left(r\,H_\phi\right)\right)\boldsymbol{e}_r + \left[\frac{\partial}{\partial z}\left(-\hat{\varepsilon_r}\frac{\partial}{\partial z}H_\phi\right) - \frac{\partial}{\partial r}\left(\frac{\hat{\varepsilon_r}}{r}\frac{\partial}{\partial r}\left(r\,H_\phi\right)\right)\boldsymbol{e}_z\right] + \frac{1}{r}\frac{\partial}{\partial\phi}\left(-\hat{\varepsilon_r}\frac{\partial}{\partial z}H_\phi\right)\boldsymbol{e}_z\right]\mathrm{e}^{j\omega t},$$

where $\hat{\varepsilon_r} = \left(\varepsilon_r - j\,\frac{\sigma}{\omega\,\varepsilon_0}\right)^{-1}$. As $\frac{\partial}{\partial\phi}H_\phi \equiv 0$, (note this is most easily calculated by Lagrange's formula for del, taking $\boldsymbol{H} = (0, H_\phi, 0)$),

$$\nabla \times \hat{\varepsilon_r}(\nabla \times \boldsymbol{H}) = -\left[\frac{\partial}{\partial z}\left[\hat{\varepsilon_r}\frac{\partial}{\partial z}H_\phi\right] + \frac{\partial}{\partial r}\left(\frac{\hat{\varepsilon_r}}{r}\frac{\partial}{\partial r}\left(r\,H_\phi\right)\right)\right]\boldsymbol{e}_\phi\,\mathrm{e}^{j\omega t}. \tag{3}$$

Hence, our governing equation becomes,

$$\left[\frac{\partial}{\partial z}\left[\hat{\varepsilon_r}\frac{\partial}{\partial z}H_\phi\right] + \frac{\partial}{\partial r}\left(\frac{\hat{\varepsilon_r}}{r}\frac{\partial}{\partial r}\left(r\,H_\phi\right)\right)\right]\boldsymbol{e}_\phi\,\mathrm{e}^{j\omega t} + \mu_r\,k_0^2\,H_\phi\,\boldsymbol{e}_\phi\,\mathrm{e}^{j\omega t} = 0.$$

Removing the oscillating term and taking the $\boldsymbol{e}_\phi$ component,

$$\left[\frac{\partial}{\partial z}\left[\hat{\varepsilon_r}\frac{\partial}{\partial z}H_\phi\right] + \frac{\partial}{\partial r}\left(\frac{\hat{\varepsilon_r}}{r}\frac{\partial}{\partial r}\left(r\,H_\phi\right)\right)\right] + \mu_r\,k_0^2\,H_\phi = 0. \tag{4}$$

This is the scalar form used in the code.

3.3.2 Scalar Variational Form

Starting from (6), we may introduce the axisymmetric, time-harmonic approximation, using a test function $\boldsymbol{T} = (0, T, 0)$,

$$\int_\Omega \left[\hat{\varepsilon_r}^{-1}\left(\frac{\partial}{\partial z}T\cdot\frac{\partial}{\partial z}H_\phi + \frac{1}{r^2}\frac{\partial}{\partial r}\left(r\,T\right)\cdot\frac{\partial}{\partial r}\left(r\,H_\phi\right)\right)\right]d\Omega$$
$$-\int_\Omega k_0^2\,\mu_r\,T\cdot H_\phi\,d\Omega = R\int_{\Gamma_1\cup\Gamma_4} T\cdot\left(2\,H_{\phi 0} - H_\phi\right)d\Gamma,$$

with the Dirichlet condition $H_\phi \equiv 0$ on Γ_3. Rearranging for linear-bilinear forms,

$$\int_\Omega \left[\hat{\varepsilon}_r^{-1} \left(\frac{\partial}{\partial z} T \cdot \frac{\partial}{\partial z} H_\phi + \frac{1}{r^2} \frac{\partial}{\partial r} (r\,T) \cdot \frac{\partial}{\partial r} (r\,H_\phi) \right) \right] d\Omega$$

$$-k_0^2\,\mu_r \int_\Omega T \cdot H_\phi\, d\Omega + R \int_{\Gamma_1 \cup \Gamma_4} T \cdot H_\phi\, d\Gamma \;=\; 2\,R \int_{\Gamma_1 \cup \Gamma_4} T \cdot H_{\phi 0}\, d\Gamma.$$

However, note that T and H_ϕ are complex, and so, for the benefit of a real variable solver, we consider the functions as maps $\mathbb{R}^2 \to \mathbb{R}^2$ to be inner-producted. This, with the Dirichlet condition $H_\phi^{\mathrm{im}} = H_\phi^{\mathrm{re}} = 0$ on Γ_3, gives us our final equation.

$$\int_\Omega \left[\hat{\varepsilon}_r^{-1} \left(\frac{\partial}{\partial z} T \cdot \frac{\partial}{\partial z} H_\phi + \frac{1}{r^2} \frac{\partial}{\partial r} (r\,T) \cdot \frac{\partial}{\partial r} (r\,H_\phi) \right) \right] d\Omega$$

$$+k_0^2\,\mu_r \int_\Omega T \cdot H_\phi\, d\Omega + R \int_{\Gamma_1 \cup \Gamma_4} T \cdot H_\phi\, d\Gamma \;=\; 2\,R \int_{\Gamma_1 \cup \Gamma_4} T \cdot H_{\phi 0}\, d\Gamma.$$

$$n \times \sqrt{\varepsilon}\, E - \sqrt{\mu} H \;=\; -2\sqrt{\mu} H_{\phi 0}$$

$$n \times \sqrt{\varepsilon_0 \varepsilon_r}\, E - \sqrt{\mu_0\,\mu_r} H \;=\; -2\sqrt{\mu_0\,\mu_r} H_{\phi 0}$$

$$\mathrm{i}\,\omega \sqrt{\varepsilon_0 \mu_0 \varepsilon_r \mu_r}\, n \times E - \mathrm{i}\,\omega\,\mu_r \mu_0 H \;=\;$$

$$\mathrm{i}\,k\,n \times E + (\nabla \times E) \;=\; ...$$

3.3.3 Expanded integrals

$$\int_\Omega \left[\hat{\varepsilon}_r^{-1} \left(\frac{\partial}{\partial z} T \cdot \frac{\partial}{\partial z} H_\phi + \frac{1}{r^2} \frac{\partial}{\partial r} (r\,T) \cdot \frac{\partial}{\partial r} (r\,H_\phi) \right) \right] d\Omega$$

$$+k_0^2\,\mu_r \int_\Omega T \cdot H_\phi\, d\Omega + R \int_{\Gamma_1 \cup \Gamma_4} T \cdot H_\phi\, d\Gamma \;=\; 2\,R \int_{\Gamma_1 \cup \Gamma_4} T \cdot H_{\phi 0}\, d\Gamma.$$

However, note that T and H_ϕ are complex, and so, for the benefit of a real variable solver, we consider the functions as maps $\mathbb{R}^2 \to \mathbb{R}^2$, with the Dirichlet condition $H_\phi^{\mathrm{im}} = H_\phi^{\mathrm{re}} = 0$ on Γ_3 giving us our final equation.

3.3.4 Expanding complex-valued functions

The assembly of the discretised problem will result in a complex coupling matrix and source term. This is due to the property $H(x) = a(x) + jb(x) = \sum_{n=1}^\infty f_n(x)a_n + j\sum_{n=1}^\infty f_n(x)b_n = \sum_{n=1}^\infty f_n(x)[a_n + jb_n] = \sum_{n=1}^\infty f_n(x)h_n$ where $f_n(x) \in \mathbb{R}$ and $h_n \in \mathbb{C}$. Solving complex system of equations in fenics requires a hack as it is not supported by default [4].

3.3.5 Vector Variational Form With Inhomogeneous Material Properties

It may be necessary to develop a full 3D model in the future and this section is included for reference, and to show the derivation of the boundary conditions. Start by multiplying the strong form in Eq. (1) by a test function $\boldsymbol{T} : \mathbb{R}^3 \to \mathbb{C}$ without loss of generality the test function can be $\boldsymbol{T} : \mathbb{R}^3 \to \mathbb{R}$ according to Section 3.3.11. The starting point is thus,

$$\int_\Omega \boldsymbol{T} \cdot [\boldsymbol{\nabla} \times \hat{\epsilon}_r (\boldsymbol{\nabla} \times \boldsymbol{H}) - \mu_r k_0^2\, \boldsymbol{H}] d\Omega = 0.$$

Using the scalar triple product identity for the divergence operator,

$$\boldsymbol{\nabla} \cdot (\boldsymbol{A} \times \boldsymbol{B}) = \boldsymbol{B} \cdot (\boldsymbol{\nabla} \times \boldsymbol{A}) - \boldsymbol{A} \cdot (\boldsymbol{\nabla} \times \boldsymbol{B}),$$

one obtains,

$$\int_\Omega [(\boldsymbol{\nabla} \times \boldsymbol{T}) \cdot \hat{\epsilon}_r (\boldsymbol{\nabla} \times \boldsymbol{H}) - \mu_r k_0^2\, \boldsymbol{H}] d\Omega = \int_\Omega \boldsymbol{\nabla} \cdot (\boldsymbol{T} \times \hat{\epsilon}_r (\boldsymbol{\nabla} \times \boldsymbol{H})) d\Omega.$$

Next apply Gauss' Theorem,

$$\int_\Omega \boldsymbol{\nabla} \cdot \boldsymbol{A}\, d\Omega = \oint_\Gamma \boldsymbol{A} \cdot \boldsymbol{n}\, d\Gamma,$$

to yield a boundary integral (which also appears to be the variational form although derived as weak form),

$$\int_\Omega [(\boldsymbol{\nabla} \times \boldsymbol{T}) \cdot \hat{\epsilon}_r (\boldsymbol{\nabla} \times \boldsymbol{H}) - \mu_r k_0^2\, \boldsymbol{H}] d\Omega = \oint_\Gamma (\boldsymbol{T} \times \hat{\epsilon}_r (\boldsymbol{\nabla} \times \boldsymbol{H})) \cdot \boldsymbol{n}\, d\Gamma.$$

The surface Γ enclosing the volume Ω is formed from the union of four types of boundary condition in this case $\Gamma = \Gamma_1 \cup \Gamma_2 \cup \Gamma_3 \cup \Gamma_4$. Let Γ_1 be the scattering boundary, Γ_2 be the conductor boundary, Γ_3 be the axisymmetric boundary and Γ_4 be the feed port.

3.3.6 First-Order Absorbing Boundary Condition (Scattering)

In order to solve the computational electromagnetic problem in a finite domain an approximation of the Sommerfeld radiation condition is required on the external boundary. A first-order absorbing boundary condition should be sufficient for this application, but if further accuracy is required a perfectly matched layer could be used [3]. The distance at which to apply any boundary condition can be determined using a sensitivity analysis. The decay of the microwaves as they propagate through tissue is significant, which may relax the requirements on the accuracy of the boundary condition.

According to Jin [3] the first-order absorbing boundary condition is given by:

$$n \times \nabla \times \boldsymbol{H} + jk_0\, n \times n \times \boldsymbol{H} \approx 0, \quad \boldsymbol{r} \epsilon \Gamma_1.$$

This can be substituted into the boundary integral and simplified,

$$\begin{aligned}
\int_{\Gamma_1} \boldsymbol{T} \times \hat{\epsilon_r}(\nabla \times \boldsymbol{H}) \cdot n\, d\Gamma &= \int_{\Gamma_1} \boldsymbol{T} \times \hat{\epsilon_r}(-jk_0(n \times \boldsymbol{H})) \cdot n\, d\Gamma, \\
&= \int_{\Gamma_1} \hat{\epsilon_r}\, jk_0(n \times \boldsymbol{H}) \times \boldsymbol{T} \cdot n\, d\Gamma, \\
&= \int_{\Gamma_1} \hat{\epsilon_r}\, jk_0(n \times \boldsymbol{H}) \cdot (\boldsymbol{T} \times n)\, d\Gamma, \\
&= -\int_{\Gamma_1} \hat{\epsilon_r}\, jk_0\, (n \times \boldsymbol{H}) \cdot (n \times \boldsymbol{T})\, d\Gamma,
\end{aligned}$$

using the vector product identities,

$$\begin{aligned}
\boldsymbol{A} \cdot (\boldsymbol{B} \times \boldsymbol{C}) &= \boldsymbol{B} \cdot (\boldsymbol{C} \times \boldsymbol{A}) \\
&\text{and} \\
\boldsymbol{A} \times \boldsymbol{B} &= -\boldsymbol{B} \times \boldsymbol{A},
\end{aligned}$$

which agrees with Jin [3].

3.3.7 Waveguide Port Boundary Condition

When modelling antennas it is sometimes necessary to model the waveguide to obtain accurate solutions [3]. It is not necessary to model the whole waveguide, just the region in the vicinity of the antenna to capture the modified modal distribution. This truncation of the feeding waveguide to form a waveguide port requires a special boundary condition. This port boundary condition is required to absorb the field reflected back into the waveguide and accurately represent the modal distribution in the waveguide region forming the antenna.

The following WPBC can be used [1]

$$\sqrt{\epsilon - j\frac{\sigma}{\omega}}\, \boldsymbol{n} \times \boldsymbol{E} - \sqrt{\mu}\boldsymbol{H_\phi} = -2\sqrt{\mu}\boldsymbol{H_{\phi 0}},$$

where $\boldsymbol{H_{\phi 0}} = (0, H_{\phi 0}, 0)^T$ and $\boldsymbol{H_\phi} = (0, H_\phi, 0)^T$. Further, note that

$$j\frac{\omega \epsilon_o}{\hat{\epsilon_r}}\boldsymbol{E} = \nabla \times \boldsymbol{H}.$$

Considering the boundary term in the variational form we can write

$$\begin{aligned}
\int_{\Gamma_1 \cup \Gamma_4} \boldsymbol{T} \times \hat{\epsilon_r}(\nabla \times \boldsymbol{H}) \cdot \boldsymbol{n}\, d\Gamma &= \int_{\Gamma_1 \cup \Gamma_4} \boldsymbol{T} \cdot (\hat{\epsilon_r}(\nabla \times \boldsymbol{H}) \times \boldsymbol{n})\, d\Gamma, \\
&= -\int_{\Gamma_1 \cup \Gamma_4} \boldsymbol{T} \cdot (\boldsymbol{n} \times \hat{\epsilon_r}(\nabla \times \boldsymbol{H}))\, d\Gamma, \\
\omega \epsilon_o \quad \text{assumed constant and factors out of curl} &= -j\omega \epsilon_o \int_{\Gamma_1 \cup \Gamma_4} \boldsymbol{T} \cdot (\boldsymbol{n} \times \boldsymbol{E})\, d\Gamma.
\end{aligned}$$

Now the boundary condition can be rewritten slightly as

$$\frac{\sqrt{\epsilon_o}}{\sqrt{\hat{\epsilon_r}}}\, \boldsymbol{n} \times \boldsymbol{E} - \sqrt{\mu}\boldsymbol{H_\phi} = -2\sqrt{\mu}\boldsymbol{H_{\phi 0}}.$$

Substituting this into the boundary term

$$
\begin{aligned}
-j\omega\epsilon_o \int_{\Gamma_1 \cup \Gamma_4} \boldsymbol{T} \cdot (\boldsymbol{n} \times \boldsymbol{E})\, d\Gamma &= -j\omega\sqrt{\mu_o}\sqrt{\epsilon_o} \int_{\Gamma_1 \cup \Gamma_4} \sqrt{\mu_r}\sqrt{\hat{\epsilon_r}}\boldsymbol{T} \cdot (\boldsymbol{H_\phi} - 2\boldsymbol{H_{\phi 0}})\, d\Gamma \\
&= -jk_o \int_{\Gamma_1 \cup \Gamma_4} \sqrt{\mu_r}\sqrt{\hat{\epsilon_r}}\boldsymbol{T} \cdot (\boldsymbol{H_\phi} - 2\boldsymbol{H_{\phi 0}})\, d\Gamma
\end{aligned}
$$

3.3.8 Verification Cases (Axisymmetric)

In this section the theory behind some of the MWA test cases is described.

Coaxial cable analytic solution

Let $H_\phi = \frac{C}{rZ}\, \mathrm{e}^{-\mathrm{i}kz}$. Then,

$$
\begin{aligned}
\nabla \times (H_\phi\, \boldsymbol{e}_\phi) &= \left(-\frac{\partial H_\phi}{\partial z}\, \boldsymbol{e}_r + \frac{1}{r}\frac{\partial}{\partial r}(r\, H_\phi)\, \boldsymbol{e}_z \right) \\
&= \frac{C}{Z}\left(\mathrm{i}\, k\, \frac{1}{r}\mathrm{e}^{-\mathrm{i}kz}\, \boldsymbol{e}_r \right) \\
\nabla \times (\nabla \times (H_\phi\, \boldsymbol{e}_\phi)) &= \frac{C}{Z}\left(k^2\frac{1}{r}\, \mathrm{e}^{-\mathrm{i}kz} \right)\boldsymbol{e}_\phi \\
&= k^2\, H_\phi\, \boldsymbol{e}_\phi \\
&= k_0^2\, \varepsilon_r\, \mu_r\, H_\phi\, \boldsymbol{e}_\phi \\
\nabla \times (\varepsilon_r^{-1}\, \nabla \times (H_\phi\, \boldsymbol{e}_\phi)) &= k_0^2\, \mu_r\, H_\phi\, \boldsymbol{e}_\phi.
\end{aligned}
$$

Trying the boundary condition,

$$
\begin{aligned}
\nabla \times H_\phi &= \frac{C}{Z}\left(\mathrm{i}\, k\, \frac{1}{r}\, \mathrm{e}^{-\mathrm{i}kz}\, \boldsymbol{e}_r \right) \\
&= \omega\left(\mathrm{i}\varepsilon\, \frac{1}{r}\, \mathrm{e}^{-\mathrm{i}kz}\, \boldsymbol{e}_r \right) \\
\Rightarrow \\
E &= \frac{1}{\mathrm{i}\,\omega\,\varepsilon}\, \nabla \times H_\phi \\
&= C\left(\frac{1}{r}\mathrm{e}^{-\mathrm{i}kz}\, \boldsymbol{e}_r \right) \\
n \times E &= (n_r\, \boldsymbol{e}_r + n_z\, \boldsymbol{e}_z) \times E \\
&= n_z\, \frac{C}{r}\mathrm{e}^{-\mathrm{i}kz}\, \boldsymbol{e}_\phi \\
&= n_z\, \frac{\sqrt{\mu}}{\sqrt{\varepsilon}}\left(\frac{C}{rZ}\mathrm{e}^{-\mathrm{i}kz}\, \boldsymbol{e}_\phi \right) \\
&= n_z\, \frac{\sqrt{\mu}}{\sqrt{\varepsilon}}\, H_\phi\, \boldsymbol{e}_\phi \\
\Rightarrow \\
\sqrt{\varepsilon}\, n \times E &= n_z\, \sqrt{\mu}\, H_\phi\, \boldsymbol{e}_\phi.
\end{aligned}
$$

To relate this to the WPBC already implemented realise from the COMSOL manual that

$$P_{\mathrm{in}} = \frac{\pi C^2}{Z}\ln(r_1/r_2) \to C = \sqrt{\frac{P_{\mathrm{in}}Z}{\pi\ln(r_1/r_2)}},$$

this allows us to test the WPBC we want to use. It appears that the first-order absorbing boundary condition is not sufficient for this problem, producing around 10% errors. If however, the WPBC is used with $H_{\phi 0} \equiv 0$ then the error becomes negligible. This makes sense as the WPBC is setting the modes of the waveguide to 0 whereas the first-order absorbing boundary condition is approximate. Conversely using the WPBC on the conc-cylinder test gives worse solutions.

Concentric Cylinders

This case consists of two concentric cylinders of biological tissues, which can have different electrical properties and sizes, with an imposed z-directional electric field. In this simple geometry an analytic solution can be derived, which is accepted without confirmation. The solution is

$$E_z(r) = A_i J_o(k_i r) + B_i Y_o(k_i r)$$

where J_o is the Bessel function of the first kind, Y_o is the Bessel function of the second kind, $k = \omega\sqrt{\mu\epsilon_o/\hat{\epsilon_r}}$, A and B are determined from the boundary conditions and the subscript i corresponds to the material properties within a particular cylinder. To obtain A and B the following system of equations must be solved

Annular Slot Antenna Test Case

This test case is based on the paper by Nevels [5]. It is a coaxially fed annular aperture antenna propagating into a lossy biological medium. The dimensions are given by products of k and the radii. This is a test of the full 2D axisymmetric domain, not a pseudo 2D case. Further it is also a test of: the WPBC, first order absorbing boundary condition, perfect electrical conductor boundary condition, symmetry condition and complex dielectric material properties. Note that the imposed TEM mode in the coaxial cable is defined as

$$E_r = \frac{V}{\ln{(b/a)}} \frac{1}{r} e^{-\mathrm{jkz}},$$

where $k = \omega\sqrt{\mu\epsilon}$, V is the applied voltage, a and b are the inner and outer radii of the coaxial respectively. In order to apply an appropriate WPBC, and ensure that the solutions correspond with those in the paper, the WPBC must be position at $z = n2\pi/k$, where n is a posotive integer. This places the boundary condition at multiples of the wavelength away from the interface with the external lossy domain. Converting this to H_ϕ gives us

$$\hat{\phi}\, H_\phi = -\frac{1}{j\omega\mu}(\boldsymbol{\nabla} \times \hat{\boldsymbol{r}})\, E_r = \frac{kV}{\omega\mu\ln{(b/a)}} \frac{1}{r} e^{-\mathrm{jkz}}.$$

Relating terms to the $H_{\phi 0}$ incident field in the Gas paper [1] and the implemented WPBC we can show that

$$H_\phi = \frac{V}{Z\ln{(b/a)}} \frac{1}{r} e^{-\mathrm{jkz}} \rightarrow C = \frac{V}{\ln{(b/a)}}$$

3.3.9 Dependencies of Dielectric Tissue Properties

In the general case we assume that the dielectric properties are given by

$$\epsilon_r(F, \mathrm{DI}, T) \text{ and } \sigma(F, \mathrm{DI}, T),$$

where F is the water content, DI is the heat damage integral, T is the temperature. The actual values of these parameters, with varying temperature, have been measured by Lapresto et al. & Ji and Brace. These measurements will implicitly capture DI and F as they were taken during MWA. The functional form used to describe the temperature dependence is

$$\eta(T) = s_1\left[1 - \frac{1}{1 + \exp{(s_2 - s_3 T)}}\right] + s_4,$$

where $\eta \in \{\epsilon_r, \sigma\}$ and s_n are parameters. It should be noted that $s_4 \in \{0, 1\}$ is not a true parameter, but in fact represents a different functional form for ϵ_r used by Ji and Brace. For this reason only parameter values for σ are probably directly comparable. The quoted values are given in the table

	s_1	s_2	s_3	s_4
ϵ_r - Ji & Brace	48.391	6.286	0.0764	1
ϵ_r - Lapresto	45.57	5.223	0.05243	0
σ - Ji & Brace	2.173	5.951	0.0697	0
σ - Lapresto	1.803	6.538	0.05984	0

3.3.10 Probes

The shape of the SAR is highly dependent on the structure of the applicator (microwave antenna) used. For this reason it is necessary to have a library of applicator models, to match those commercially available, even in axisymmetric coordinates. Currently these are implemented in test cases and includes:

1. Annular slot antenna (Gas),

2. Coaxial monopole (Ji and Brace),

3. AMICA (prototype 1),

4. AMICA (prototype 2).

3.3.11 Code Parameters

The relevant code variables for the equations derived in this section are given in Tab. 3. There are examples of setting up a static computation of the SAR for MWA in tosoratti-2003.py and tosoratti-2011.py.

Symbol	Variable Name	Description
ω	om	angular frequency
P_{in}	Pin	applied applicator power
r_1	r_1	inner radius coax feed line
r_2	r_2	outer radius coax feed line
$\text{Re}(H_{\phi 0})$	H_phi_0_re	real component of the coax fundamental mode
$\text{Im}(H_{\phi 0})$	H_phi_0_im	imaginary component of the coax fundamental mode
ϵ_r	eps_r_by_subdomain	relative permittivity
σ	sigma_by_subdomain	effective conductivity
μ_r	mu_r_by_subdomain	relative permeability
C	C_dielectric	parameter of waveguide port boundary condition
Z	Z_dielectric	parameter of waveguide port boundary condition
s_1	es1 / ss1	parameter of sigmoidal form of ϵ_r / σ
s_2	es2 / ss2	parameter of sigmoidal form of ϵ_r / σ
s_3	es3 / ss3	parameter of sigmoidal form of ϵ_r / σ
s_4	es4 / ss4	parameter of sigmoidal form of ϵ_r / σ

Table 3.

3.4 Cell Death Model (RFA & MWA)

The cell death model that has been implemented is that of O'Neill et al. The parameters are set, by default, to the optimal values given in Tab. 2 of the paper. The cell death model is solved for every nodal point in the finite element mesh, over the current time step, to produce a scalar field representing the cell viability vs time. To turn on the cell death model a flag must be set cda_update = True.

In order to stop the perfusion during a calculation, as a result of damage to the vasculature, the parameter perf_model = "stop" must be set. This corresponds to a viability <0.8.

4 Test Cases

In order to perform code verification, a collection of test cases has been assembled that will eventually cover all implemented features. This is a collection of problems with analytic solutions, manufactured solutions and results from the literature.

4.1 Solidification due to line heat sink

File: 1d-solidification-test.py

Status: working

Description: this test case sets up a line heat sink at $r = 0$ in a domain initially at 310K and then models the phase change as a function of time. An analytic solution is available for this problem, which is computed and stored in the file analytic.pvd.

Expected Result: the predicted temperature profile in enthalpy.pvd should agree closely with that in analytic.pvd. Further, numerical predictions of the interface location (defined as Tu>T>Tl) should coincide with the analytic solution at all times.

4.2 Cell death test

File: cell-death-test.py

Status: working

Description: this test case runs a transient calculation with a fixed homogeneous temperature. This is to allow comparison of the implemented cell death ODE solver with a standard adaptive ODE solver.

Expected Result: V should agree with the solutions generated by cell_death_test.m in the matlab directory. The matlab results are stored in matlab.pvd for easy comparison in paraview.

4.3 Concentric cylinder test

File: conc-cyl-test.py

Status: working

Description: this test case imposes an electric field on the outer surface of two concentric cylinders of tissue. An analytic solution exists for this situation and the comparison is performed and results displayed graphically and on the command line.

Expected Result: The L2 norm error should be low and the second plot should be close to zero in the middle of the domain (not throughout due to boundary conditions at cylinder ends).

4.4 Method of Manufactured solutions steady-state Pennes equation

File: mms-heat-only-test.py

Status: working

Description: this test case uses the method of manufactured solutions to test that steady state solutions to the Pennes equation can be successfully computed.

Expected Results: The L2 norm error should be low, the error is plotted in T-error.pvd.

4.5 Method of Manufactured solutions transient nonlinear Pennes equation

File: mms-heat-only-nonlinear.py

Status: working

Description: this test case uses the method of manufactured solutions to test the transient nonlinear capabilities of fenics_mwa.

Expected Results: The L2 norm error should be low, the temperature profiles should agree at all times.

4.6 Transient Laser Heating Benchmark

File: vyas-1992.py

Status: working

Description: this test case involves a laser source in tissue to provide heat that is only active for an initial period and then switched off [7]. The source is provided as an SAR, and therefore this tests the transient linear Pennes equations solution. There is an analytic solution and this is used for comparison.

Expected Results: The publication uses a cross section of the temperature at a specific time point to evaluate the solution accuracy.

4.7 Single Tine RFA

File: single-tine-sym-rfa.py

Status: working

Description: this test case is going to be the base of the RFA sensitivity study. For this reason it has all of the nonlinearities present and the impedance based control system switched on. It is based on the test case used by Trujillo et al. cite{Trujillo2012} which has some example solutions and experimental data for comparison.

Expected Results: Currently expect code to converge to a solution with physically reasonable temeprature and cell death predictions.

4.8 Single Tine RFA convergence tests

File: single-tine-sym-rfa-conv.py

Status: working

Description: this test runs through a variety of meshes of increasing resolution to determine the mesh sensitivity. The total mesh volume is also increased to see if there is a dependence on this.

Expected Results: array of convergence of max and min field quantities.

4.9 Annular Slot Antenna

File: gas-probe-sensitivity.py

Status: working

Description: this test case implements the MWA applicator specified in Gas et al.

Expected Results: -

4.10 Temperature Dependent Electrical Properties (MWA)

File: ji-brace-2011.py

Status: working

Description: this test case evaluates temperature dependent electrical properties specified in Ji & Brace cite{Ji2011}. This problem is nonlinear and therefore needs small timesteps. Very clear difference can be seen between a constant value and temperature dependence.

Expected Results: Should agree with results in paper.

4.11 AMICA Prototype 2003

File: tosoratti-2003.py

Status: working

Description: computes the SAR for the AMICA prototype.

Expected Results: Should agree with results in paper.

4.12 AMICA Prototype 2003 Comparison

File: tosoratti-2003-unchoked.py

Status: working

Description: computes the SAR for the comparison unchoked applicator to show the difference.

Expected Results: Should agree with results in paper.

4.13 AMICA Prototype 2011

File: tosoratti-probe-2011.py

Status: working

Description: computes the SAR for the AMICA prototype.

Expected Results: Should agree with results in paper.

4.14 Future Test Cases

1. RD Nevels
2. MMS nonlinear system

5 Implementation Notes

Various implementation issues inevitably arise when developing a code of this type. These are detailed here for reference.

5.1 Parameter Dependencies

There are a variety of functional forms for the dependencies of the model parameters proposed in the literature. Many of these vary spatially through their dependence on temperature or cell viability and can pose a computational issue as a result of the polynomial basis in FEM. The dramatic drop in conductivity as the temperature approaches 373K can occur in the middle of an element leading to negative values of the interpolating polynomials.

For this reason the state variable e.g. temperature is projected onto a discontinuous galerkin (DG) order 0 function space before evaluating the dependent parameter e.g. σ. This ensures that no negative values are erroneously generated. It also ensures that the parameter values are piecewise constant, which is compatible with FEM. The fine mesh in the areas where these effects are observed along with the size of the inherent uncertainties in the parameter values mean that this approach should not impact the solution accuracy greatly.

5.2 Nedelec Elements in MWA

Lagrange finite elements are not appropriate for the solution of Maxwell's Equations due to the interference as a result of spurious modes. To address this Nedelec elements need to be used in their place. These are a standard option in FEniCS.

5.3 Strang Splitting

The final system of equations for RFA and MWA includes PDEs describing the transfer of heat and the electric field and a system of ODEs describing the cell death. In order to solve this system of nonlinear equations an *ad hoc* linearisation has been performed. It should be possible to improve this in the future using operator splitting, which can generate iterative schemes for this type of problem. This type of method is commonly employed to solve the bidomain equations in cardiac modelling.

5.4 git Repository Details

The branching model used is available here: http://nvie.com/posts/a-successful-git-branching-model/ (19/09/14). The develop branch will always be kept on a local machine and will be the most complete version containing files not available on the master branch. The master branch will be published online on github to allow users to access working copies and to start making their own modifications. If the need arises, the develop branch can be posted online for collaboration. The url for the master branch on github is:

  https://github.com/sheldonkhall/MITA-model.git

The release branch will normally contain a subset of the develop branch and therefore care must be taken when performing a merge. Essentially, when merging a bugfix performed in the feature branch into the develop branch the ours merge strategy must be selected. The command is:

  git checkout develop
  git merge –no-f -s ours release

This should stop files removed for the release being removed from the develop branch.
  When preparing a release the command:

  git clean

is useful for removing untracked (automatically generated) files. This will NOT remove .pyc files however and these may cause problems when not doing a fresh install.
  In order to list all deleted files (useful when merging changes from hotfix and release back to develop use:

  git log –diff-filter=D –summary

  In order to keep the online repository clean: a new branch was created. This is called trunk and will contain the released publically available code. This is stripped of the history during creating by using the command:

  git checkout –orphan trunk

then trunk is merged with release. This branch can then be pushed to github and lacks the unneeded develop history.

Bibliography

[1] Piotr Gas. Temperature Distribution of Human Tissue in Interstitial Microwave Hyperthermia. *PRZEGLĂDD ELEKTROTECHNICZNY* , 88(7a):144–146, 2012.

[2] Dieter Haemmerich, Louay Chachati, Andrew S Wright, David M Mahvi, Fred T Lee and John G Webster. Hepatic radiofrequency ablation with internally cooled probes: effect of coolant temperature on lesion size. *IEEE transactions on bio-medical engineering*, 50(4):493–500, apr 2003.

[3] Jian-Ming Jin and Douglas J. Riley. *Finite Element Analysis of Antennas and Arrays*. John Wiley & Sons, 2009.

[4] Neilen Marais. Electrical Dipole and First Order Absorbing Boundary Condition (ABC) with Dolfin. 2011.

[5] R.D. Nevels, C.M. Butler and W. Yablon. The Annular Slot Antenna in a Lossy Biological Medium (Short Papers). *IEEE Transactions on Microwave Theory and Techniques*, 33(4):314–319, apr 1985.

[6] Macarena Trujillo and Enrique Berjano. Review of the mathematical functions used to model the temperature dependence of electrical and thermal conductivities of biological tissue in radiofrequency ablation. *International journal of hyperthermia : the official journal of European Society for Hyperthermic Oncology, North American Hyperthermia Group*, , jul 2013.

[7] Reeta Vyas. GreenâĂŹs function solution to the tissue bioheat equation. *Medical Physics*, 19(5):1319, sep 1992.